Salient feature of haptic based guidance of people in low visibility environments using hard reins

Anuradha Ranasinghe, Prokar Dasgupta, Kaspar Althoefer, *Member, IEEE,* Jacques Penders,
and Thrishantha Nanayakkara, *Member, IEEE*

Abstract—This paper presents salient features of human-human interaction where one person with limited auditory and visual perception of the environment (a follower) is guided by an agent with full perceptual capabilities (a guider) via a hard rein along a given path. We investigate several salient features of the interaction between the guider and the follower such as a) the order of an autoregressive control policy that maps states of the follower to actions of the guider, b) how the guider may modulate the pulling force in response to the confidence level of the follower, and c) how learning may successively apportion the responsibility of control across different muscles of the guider. Based on experimental systems identification on human demonstrations from ten pairs of naive subjects, we show that guiders tend to adopt a 3rd order auto-regressive predictive control policy and followers tend to adopt 2nd order reactive control policy. Moreover, the extracted guider's control policy was implemented and validated by human-robot interaction experiments. By modeling the follower's dynamics with a time varying virtual damped inertial system, we found that it is the coefficient of virtual damping which is most sensitive to the confidence level of the follower. We used these experimental insights to derive a novel controller that integrates an optimal order control policy with a push/pull force modulator in response to the confidence level of the follower monitored using a time varying virtual damped inertial model.

Index Terms—Human robot interaction, hard rein, haptic communication, predictive and reactive control policies.

I. INTRODUCTION

HAPTIC perception is a natural solution for humans when vision is impaired. This paper presents identification of abstracted dynamics of human control policies to guide/follow using a hard rein in low visibility conditions. These results allow to identify control policies for the structure of motor controllers used by human participants to guide a blindfolded counterpart. The extracted haptic-based guidance policies can be implemented on a robot to guide a human in low visibility conditions like in indoor fire-fighting, disaster response, and search and rescue operations [1], [2].

Several attempts have been made on guiding people with visual and auditory impairments using intelligent agents in cases such as fire-fighting [3] and guiding blind people using guide dogs [4]. However, our intention is to derive guiding/following control policies based on human-human demonstrations to be used in a robot to guide people with good vision working in

Anuradha, Kaspar, and Thrishantha are with Centre for Robotic Research, Department of Informatics, King's College London, UK

Jacques is with Sheffield Centre for Robotics, Sheffield Hallam University, UK.

Prokar is with MRC Centre for Transplantation, DTIMB & NIHR BRC, King's College London, UK.

low visibility environments. Fire-fighters have to work in low visibility conditions due to smoke or dust and high auditory distractions due to their oxygen masks and other sounds in a typical fire-fighting environment. Nowadays, they depend on touch sensation (haptic) of walls for localizing and ropes for finding the direction [3]. This paper explores how to model control policies for guiding/following by a simple Auto Regressive model (AR) when vision is limited.

There have been some studies on guiding humans to provide navigation aids when the vision was impaired [4], [5]. A robotic guide dog with environment perception capabilities called Rovi has been developed [6] to guide a human with limited environment perceptions. Rovi could avoid obstacles and reach a target on a smooth indoor floor, however difficulties arise in uncertain environments. An auditory navigation support system for the blind is discussed in [5], where, visually impaired human participants (blind folded participants) were given verbal commands by a speech synthesizer. However, speech synthesis is not a good choice to command a person in a stressful situation like a real fire. Ulrich *et al* [7] developed a guide cane without acoustic feedback in 2001 [7]. The guide cane has an ability to analyze the situation and determines appropriate direction to avoid the obstacle, and steers the wheels without requiring any conscious effort [7]. A robotic guide called MELDOG was designed by Tachi *et al* [8] to introduce effective mobility aids for the blind people. Moreover, Loomis *et al* [9] developed a personal navigation system to guide blind people in familiar and unfamiliar environments.

However, all of these studies in [3] - [9] were designed to provide navigation aids in structured environments in low visibility conditions. We show how to extract control policies of the guider and the follower when the follower's vision is impaired. Although extensive research has been carried out on navigation and path finding for a human with limited perception, to the best of our knowledge no work has been done to cover state dependent bi-directional control action for guiding them.

So far, there has been little discussion about human confidence on robots in unstructured environments. Confidence is one of the most critical factors in urban search and rescue missions because it can impact the decisions human make in uncertain conditions [10]. We argue that any robotic assistant to a person with limited perception of the environment should monitor the level of confidence of the person to be relevant to the psychological context of the person being assisted. Few attempts have been made to study confidence of a human with limited perception [11], [12] in different environments. In a

simulated game of fire-fighting, Stormont *et al* [11] showed that the fire-fighters become increasingly dependent upon robotic agents when the fire starts to spread along randomly changing in wind directions. Freedy [12] has discussed how self confidence correlates with trust of automation in human robot collaboration. Moreover, [13], [10] studied how human trust can be explained quantitatively. However, our attempt is not only to quantify the human confidence but also to model it in real time. Therefore, in this paper we discuss a novel optimal state-dependent controller that accounts for the level of confidence of the follower as part of the state.

The paper is organized as follows. Section II elaborates the experimental methodology to collect data of human-human interactions via a hard rein while tracking an arbitrary path. Section III describes the mathematical model of the guider's and the follower's state dependent control policy. Section IV gives the experimental results of human participants along with numerical simulation results to show the stability of the control policy identified through experiments. It also discusses the virtual time varying damped initial model to estimate the confidence of the human follower. Moreover, it discusses the validation of the guider's control policy extracted from human demonstration experiments. Finally, Section V concludes with the discussion.

II. Experimental Methodology

We conducted three separate experiments to understand: 1) The state dependent control policy of human subjects when one human is guiding another human with limited visual and auditory environmental perceptions in an arbitrary complex path, 2) To model the confidence level of the follower using a time varying damped initial system, and 3) To validate the guider's control policy.

A. Experimental protocol

1) Experiment 1: Extraction of control policies.: The first experiment was conducted to extract control policies in guiding/following with ten pairs of subjects after giving informed consent. They were healthy and in the age group of 23 - 43 years. Fig. 1(A) shows how the guider and the follower held both ends of hard rein to track the wiggly path. Fig. 1(A) shows the follower was blindfolded and cutoff from using auditory feedback. Fig. 1(B) shows the relative orientation difference between the guider and the follower (referred to as state hereafter), and angle of the 0.7m long, 500g weight rein relative to the agent (referred to as action hereafter).

For clarity, the detailed wiggly path is shown in Fig. 1(C). The path of total length 9m was divided into nine milestones as shown in Fig. 1(C). In any given trial, the guider was asked to take the follower from one milestone to another at six milestones up or down (ex. 1-7, 2-8, 3-9, 9-3, 8-2, and 7-1). The starting milestone was pseudo-randomly changed from trial to trial in order to eliminate the effect of any memory of the path. Moreover, the guider was disoriented before starting every trial. The guider was instructed to move the handle of the hard rein only on the horizontal plane to generate left and right turn commands. Furthermore, the guider was instructed to use push and pull commands for forwards and backwards movements to track the follower in the defined path as shown in Fig. 1(C). The follower was instructed to pay attention to the commands via the hard rein to follow the guider. The follower started to follow the guider once a gentle tug was given by the guider via the rein. The subjects were asked to maintain a natural speed of walking during the trial.

2) Experiment 2: Model the confidence of the follower.: A second experiment was conducted to study how to model the confidence of the follower in different path tracking context. There were 10 trials each for three different paths as shown in Fig. 1(D). ATI Mini40 6-axis force torque transducer was attached to the hard rein to measure tug force sampled at 1000Hz along the horizontal plane to guide the follower. The acceleration of the follower was measured by MTx sensors as shown in Fig. 1(C).

To study the confidence from the human follower, a confidence scale 1 to 10 ranging from lowest to highest was introduced before starting the experiments and subjects were asked to rate their confidence to follow the guider after the each trial.

3) Experiment 3: Implementation and validation of the guider's control policy.: The aim of the third experiment is to validate the guider's control policy when it was implemented on a planar 1-DoF freedom robotic arm. We show how the guider's control policy would bring the follower into the desired position when we replicated human-human demonstration set up in Fig. 1(B) by human-robot interaction experiments as shown in Fig. 1 (E). The guiders arm was replaced by planar 1-DoF robotic arm to generate the swing arm action in horizontal plane as shown in Fig. 1 (F). The hard rein held by the human follower connected to the robotic arm across a passive joint. The guiders control policy in Eq. 2 was imported to generate a tug force in horizontal plane. The planar 1-DoF robotic arm was actuated by a motor.

Here the cord was attached to the waist belt of the blindfolded subjects and the encoder on the shaft platform as shown in Fig. 1 (F). The subjects were instructed to move proportionally to the force they felt and to the direction of the tug force. Once the trial was started, the encoder mounted on the motor shaft read instantaneous error ϕ of the blindfolded subject's position relative to the desired angle. We defined $-65°$, $-45°$, $-25°$, $+25°$, $+45°$ and $+65°$ as desired angles. Then the robotic arm computed the commands to perturb the arm to minimize the following error between the human subject and the robotic arm. We conducted experiments with 8 subjects. Each subject participated in three trials.

B. Sensing

MTx motion capture sensors (3-axis acceleration, 3-axis magnetic field strengths, 4-quaternions, 3-axis Gyroscope readings (Xsens,USA)) were used to measure the states ϕ and actions θ of the duo. Two MTx sensors were attached on the chest of the guider and the follower to measure the rate of change of the orientation difference between them (state). Another two motion trackers attached on the hard rein to measure the angle of the rein relative to the sensor
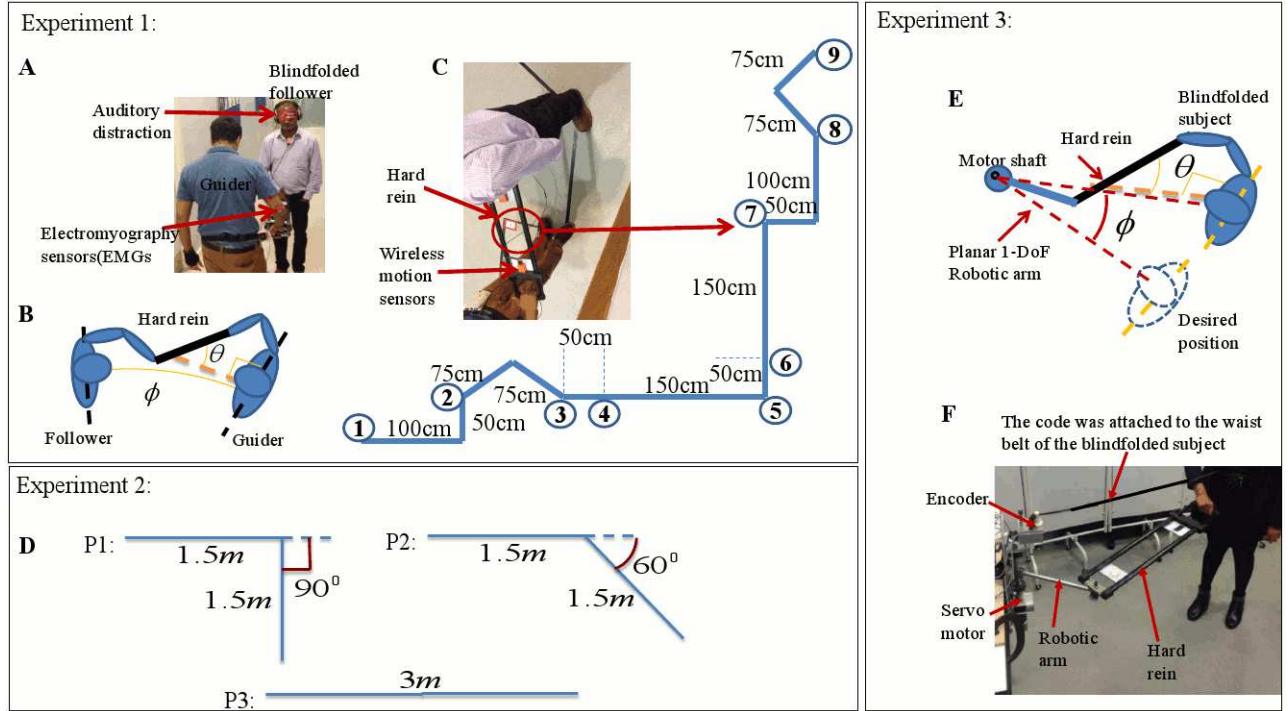
Fig. 1. The experimental setup: Experiment 1: (A) Pushing/pulling in horizontal plane to guide the follower, (B) Tracking the path by the duo, (C)The detailed diagram of labeled wiggly path on a floor, the hard rein with wireless MTx motion sensors attached to measure the state ϕ and the action θ. Experiment 2: (D) The three different paths for confidence stuies to measure pushing/pulling force in paths, P1: Ninety degree turn, P2: Sixty degree turn, and P3: Straight path. Experiment 3: (E) Schematic diagram: Human-human experimental setup in Fig. 1(B) was replicated by human-robot experimental setup. The guiders arm was replaced by planner 1-DoF robotic arm to generate the swing arm action in the horizontal plane. The hard rein held by the human follower connected to the robotic arm across a passive joint. Here, ϕ the is relative orientation difference between the motor shaft and the guider and θ is the swing action in horizontal plane., (F) The experimental setup: The cord was attached to the waist belt of the blindfolded subjects and the encoder on the shaft platform to measure the relative error.

on the chest of the guider (action from the guider). Four Electromyography (EMG) electrodes at 1500Hz were fixed on the guider's Anterior Deltoid, Biceps, Posterior Deltoid and Lateral Triceps along the upper arm as shown in Fig. 1(A). Before attaching EMG electrodes, the skin was cleaned with alcohol. An extra motion tracker with a switch was worn by the guider. To synchronize MTx motion sensors with muscle EMG sensors, we achieved this synchronization by serially connecting a channel of the EMG recorder with the magnetic sensor of the MTx sensor via a switch. the guider switched on the circuit, it induced a magnetic pulse in the MTx motion sensor while recording a voltage pulse in one of the channels of the EMG records. Since we used five MTx sensors, we sampled data at 25Hz to stay within hardware design limits.

C. Data Analysis

All data were analyzed using MATLAB R2012a (The Math Works Inc). We used Daubechies wave family (db10) of the MATLAB Wavelet Toolbox to extract the action of the guider and the state of the follower. Symlet wave family (sym8) of MATLAB was used for EMG analysis. All statistical significances were computed using the Mann-Whitney U test.

The experimental protocol was approved by the King's College London Biomedical Sciences, Medicine, Dentistry and Natural and Mathematical Sciences research ethics committee.

III. MODELING

A. The guider's closed loop control policy

We model the guider's control policy as a N-th order state dependent discrete linear controller. The order N depends on the number of past states used to calculate the current action.

Let the state be the relative orientation between the guider and the follower given by ϕ, and the action be the angle of the rein relative to the sensor on the chest of the guider given by θ as shown in Fig. 1(B). Then the linear discrete control policy of the guider is given by

$$\theta_g(k) = \sum_{r=0}^{N-1} a_r^{gRe}\phi_g(k-r) + c^{gRe} \quad (1)$$

if it is a reactive controller, and

$$\theta_g(k) = \sum_{r=0}^{N-1} a_r^{gPre}\phi_g(k+r) + c^{gPre} \quad (2)$$

if it is a predictive controller, where, k denotes the sampling step, N is the order of the polynomial, $a_r^{gRe}, a_r^{gPre}, r = 1,2,\cdots,N$ is the polynomial coefficient corresponding to the r-th state in the reactive and predictive model respectively, and c^{gRe}, c^{gRe} are corresponding scalars.

B. The follower's state transition policy

While the guider's control policy is represented by Eqs. (1) and (2), we again model the follower's control policy as an N-th order action dependent discrete linear controller to understand behavior of the follower. The order N depends on the number of past actions used to calculate the current state. Then the linear discrete control policy of the follower is given by

$$\phi_f(k) = \sum_{r=0}^{N-1} a_r^{fRe} \theta_f(k-r) + c^{fRe} \qquad (3)$$

if it is a reactive controller, and

$$\phi_f(k) = \sum_{r=0}^{N-1} a_r^{fPre} \theta_f(k+r) + c^{fPre} \qquad (4)$$

if it is a predictive controller, where, k denotes the sampling step, N is the order of the polynomial, $a_r^{fRe}, a_r^{fPre}, r = 1, 2, \cdots, N$ is the polynomial coefficient corresponding to the r-th state in the reactive and predictive model respectively, and c^{fRe}, c^{fPre} are corresponding scalars. These linear controllers in Eqs. (1), (2), (3), and (4) can be regressed with the experimental data obtained in the guider-follower experiments above to obtain the behavior of the polynomial coefficients across trials. The behavior of these coefficients for all human participants across the learning trials will give us useful insights as to the predictive/reactive nature, variability, and stability of the control policy learned by human guiders. Furthermore, a linear control policy given in Eqs. (1), (2), (3), and (4) would make it easy to transfer the fully learned control policy to a robotic guider in a low visibility condition.

C. Modeling the follower as a virtual time varying damped initial system

In order to study how the above control policy would interact with the follower in an arbitrary path tracking task, we model the voluntary following behaviour of the blindfolded human participant (follower) as a damped inertial system, where a force $F(k)$ applied along the follower's heading direction at sampling step k would result in a transition of position given by $F(k) = M\ddot{P}_f(k) + \zeta \dot{P}_f(k)$, where M is the virtual mass, P_f is the position vector in the horizontal plane, and ζ is the virtual damping coefficient. It should be noted that the virtual mass and damping coefficients are not those real coefficients of the follower's stationary body, but the mass and damping coefficients felt by the guider while the duo is in voluntary movement. This dynamic equation can be approximated by a discrete state-space equation given by

$$x(k+1) = Ax(k) + Bu(k) \qquad (5)$$

where, k is the sampling step, $x(k+1) = \begin{bmatrix} P_f(k+1) \\ P_f(k) \end{bmatrix}$,

$A = \begin{bmatrix} (2M+T\zeta)/(M+T\zeta) & -M/(M+T\zeta) \\ 0 & 0 \end{bmatrix}$,

$B = \begin{bmatrix} T^2/(M+T\zeta) \\ 0 \end{bmatrix}$,

and T is the sampling time.

Given the updated position of the follower $P_f(k)$, the new position of the guider $P_g(k)$ can be easily calculated by imposing the constraint $\|P_f(k) - P_g(k)\| = L$, where L is the length of the hard rein. Once the parameters of the Eq. 2 are known, the damped inertial model of the voluntary movement of the follower can be combined to form a complete state dependent controller that accounts for the confidence level of the follower as given by $\begin{bmatrix} F(k+1) \\ \theta(k+1)) \end{bmatrix} = \begin{bmatrix} 1 & 0 \\ 0 & 1 \end{bmatrix} \begin{bmatrix} F(k)) \\ \theta(k) \end{bmatrix} + \begin{bmatrix} (M-M_0)\ddot{P}_f(k) - (\zeta-\zeta_0)\dot{P}_f(k)) \\ \sum_{r=0}^{N-1} a_r^{Pre}\phi(k+r) + C^{Pre} \end{bmatrix}$ Where M_0 and ζ_0 are desired mass and desired damping coefficients respectively. This complete state dependent controller can be readily implemented in a potential human-robot interaction scenario.

IV. EXPERIMENTAL RESULTS

We conducted experiments with human participants to understand how the coefficients of the control policy relating states ϕ and actions θ given in Eqs. (1), (2), (3), and (4) settle down across learning trials. In order to have a deeper insight into how the coefficients in the discrete linear controller in Eqs. (1), (2), (3), and (4) change across learning trials, we ask 1) whether the guider and the follower tend to learn a predictive/reactive controllers across trials, 2) whether the order of the control policy of the guider in Eqs. (1) and (2) and the order of the control policy of the follower in Eqs. (3) and (4) change over trials, and if so, what its steady state order would be.

A. Adoption of Wave families for action and state vector profiles

To find regression coefficients, since the raw motion data were contaminated with noise, we used Wavelet Toolbox (The Math Works Inc) to extract the action and the state from raw data. The guiders action in horizontal plane is likely swing. It was suggested to adopt the Daubechies wave family (for sinusoidal waves) [14]. Moreover, according to the previous studies [15], [16], human arm movements are continuous and smooth. Therefore, a continuous mother wavelet (db10) is taken to represent the swing actions in wavelet analysis as shown in Fig. 2(A). For clarity, we compared the percentage of db10 and harr wave families for the same vector as shown in Fig.2(A). Considering previous studies and wave families comparison as shown in Fig. 2(A), we select db10 (Daubehies) for our swing type action analysis.

Different decompression levels were tested for db10. The percentage of energy corresponding to approximation for different decomposition levels were found to be 99.66%, 93.47%, and 86.73% for decompression levels 4, 8, and 15 respectively. The highest percentage of energy was gained when the decompression levels are 4. Therefore we decided to use decompression level 4 for our analysis.

To find the decomposition level from 4th decompression level, we show that the vector contains the percentages of energy corresponding to the level 4 as shown in Fig. 2(B). Considering the percentage values of 1st to 4th decomposition
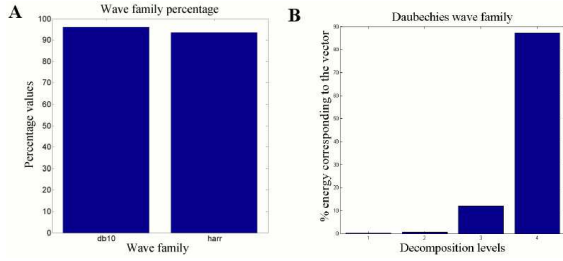
Fig. 2. Selection of wavelet family for guiding agent action and state vectors:(A) Two wavelet families (db10, harr) energy percentage representation of action vector of all subjects in all trials. (B) Vector containing the percentages of energy corresponding to the details of energy percentage of db10.

values in Fig 2(B), the highest percentage, 88% (4th decomposition level) was chosen for action and state vector analysis.

TABLE I
GUIDER PREDICTIVE $\triangle R^2\%$ OF 2nd TO 4th ORDER POLYNOMIALS W.R.T 1st ORDER. STATISTICAL SIGNIFICANCE WAS COMPUTED USING THE MANN-WHITNEY U TEST.

Trial No:	2nd order	3rd order	4th order	p values
4	8.94	11.37	11.97	
8	8.26	10.98	11.62	
12	7.81	10.36	10.74	$p\left(2^{nd} \leftrightarrow 3^{rd}\right) < 0.008^*$,
16	9.38	11.68	12.25	$p\left(3^{rd} \leftrightarrow 4^{th}\right) > 0.5$
20	9.74	14.00	14.70	

TABLE II
FOLLOWER REACTIVE $\triangle R^2\%$ OF 2nd TO 4th ORDER POLYNOMIALS W.R.T 1st ORDER. STATISTICAL SIGNIFICANCE WAS COMPUTED USING THE MANN-WHITNEY U TEST.

Trial No:	2nd order	3rd order	4th order	p values
4	8.58	9.57	9.91	
8	8.31	10.33	10.77	
12	7.41	8.46	8.70	$p(2^{nd} \leftrightarrow 3^{rd}) > 0.1$,
16	9.45	10.21	10.51	$p(3^{rd} \leftrightarrow 4^{th}) > 0.5$
20	9.96	11.82	12.29	

B. Determination of the salient features of the guider's control policy

Hereafter, the 4th decomposition level of db10 of action θ and state ϕ vectors were used for regression in Eqs. (1) and (2). Once the coefficients of the polynomial in Eqs. (1) and (2) are estimated, the best control policy (Eqs. (1) or (2)), and the corresponding best order of the polynomial should give the best R^2 value for a given trial across all subjects. Here, twenty experimental trials were binned to five for clarity.

1) Determination of predictive \ reactive nature of the guider's control policy: To select best fit policies, coefficients of (Eqs. (1) are (2)) were estimated from 1st order to 4th order polynomials shown in Fig. 3(A). Dashed line and solid line were used to denote reactive and predictive models respectively. From Fig. 3(A), we can notice that the R^2 values corresponding to the 1st order model in both Eqs. (1) and (2) are the lowest. The relatively high R^2 values of

the higher order models suggest that the control policy is of order > 1. Therefore, we take the percentage (%) differences of R^2 values of higher order polynomials relative to the 1st order polynomial for both Eqs. (1) and (2) to assess the fitness of the predictive control policy given in Eq. (2) relative to the reactive policy given in Eq. (1). Fig. 3(B) shows that the marginal percentage (%) gain in R^2 value (%ΔR^2) of 2nd, 3rd, and 4th order polynomials in Eq. (2) predictive control policy, (solid line) grows compared to those of the reactive control (dashed line) policy in Eq. (1). Therefore, we conclude that the guider gradually gives more emphasis on a predictive control policy than a reactive one.

2) Determination of the model order of the guider's control policy: The percentage (%) gain of of 3rd order polynomial is highest compared to 2nd and 4th order polynomials as shown in Table I by numerical values and the Fig. 3(B). There is a statistically significant improvement from 2nd to 3rd order models ($p < 0.008$), while there is not significant information gain from 3rd to 4th order models ($p > 0.5$). It means that the guider predictive control policy is more explained when the order is $N = 3$. Therefore, hereafter, we consider 3rd order predictive control policy to explain the guider's control policy. Moreover, individual guider's predictive/reactive nature and the model order selection are shown in the tree diagram in Fig. 3(E).

C. Determination of the salient features of the follower's policy

Next we try to understand the salient features of the follower's state transition policy in response to guider's actions, hereafter referred to as follower's policy.

1) Determination of predictive/reactive nature of the follower's control policy: We used experimental data for state θ and action ϕ in Eqs. (3) and (4) to extract features of the follower's policy from 1st to 4th order polynomials over trials as shown in Fig. 3(C). Here, we used same mathematical and statistical method as guider's model. Interestingly, Fig. 3(C) shows that the marginal percentage (%) gain in R^2 value (%ΔR^2) of 2nd, 3rd, and 4th order polynomials in Eq. (3) reactive control policy, (dashed line) grows compared to those of the predictive control policy (solid line) in Eq. (4). Therefore, we conclude that the follower gradually gives more emphasis on a reactive policy than a predictive one.

2) Determination of the model order of the follower's control policy: We tried to find the best fit order to explain the follower's policy. The percentage (%) gain of of 2nd order polynomial is highest compared to 3rd and 4th order polynomials as shown in Table II by numerical values and the Fig. 3(D). Interestingly, There is no statistically significant improvement from 2nd to 3rd order models ($p > 0.1$) nor from 3rd to 4th order models ($p > 0.5$). Therefore, we can say the follower reactive policy is more explained when the order is $N = 2$. Therefore, hereafter, we consider 2nd order reactive policy to explain the follower's policy. For clarity, individual followers predictive/reactive nature and the model order selection are shown in the tree diagram in Fig. 3(F). Our interpretations as to why the follower's autoregressive reactive policy is a 2nd
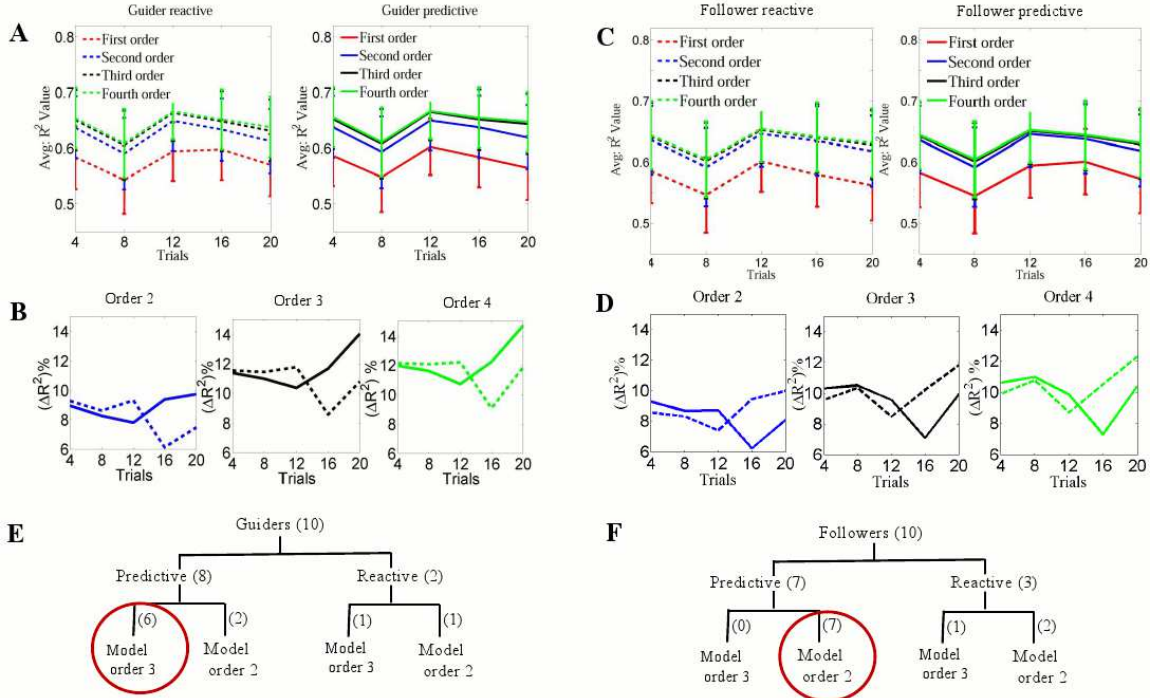
Fig. 3. R^2 values from 1st order to 4th order polynomials for the guider and the follower: reactive models (dashed line) and predictive models (solid line): (A) and (C) are the R^2 value variation of the reactive and predictive from 1st to 4th order polynomials over trials for the guider and the follower respectively. (B) and (D) are the percentage (%) differences of R^2 values of 2nd to 4th order polynomials with respect to 1st order polynomial for the guider's and the follower's control policies respectively: 2nd order, 3rd order , 4th order, (E) Individual guider's model orders and the predictive/reactive nature distribution by a tree diagram. The guider is most likely on 3rd order predictive and (F) Individual follower's model orders and the predictive/reactive nature distribution by a tree diagram. The follower is most likely on 2rd order reactive models.

one, whereas the guider's autoregressive predictive policy in a 3rd or higher order is that a reactive behavior does not need as many past states as in a predictive behavior to take action.

D. Polynomial parameters of autoregressive state dependent behavioral policies of the duo

Then we move onto understand how the polynomial parameters of the guider's 3rd order predictive and the follower's 2nd order reactive policies would evolve across learning trials in Eqs. (2) and (3) for the guider and the follower respectively. We notice in Figs. 4 and 5 that the history of the polynomial coefficients fluctuates within bounds for both the guider predictive and the follower reactive (The average and standard deviation (denoted by avg: and std: respectively) values of the coefficients are labeled in Figs. 4 and 5). This could come from the variability across participants and variability of the parameters across trials itself. Therefore, we estimate the above control policy as a bounded stochastic decision making process.

E. Modeling the follower's confidence level in different paths

Here our intention is to incorporate the instantaneous confidence level of the follower in the state-space of the closed loop controller. We show the results of variability of voluntary movements of a blindfolded follower in a haptic based guidance scenario, in a virtual damped inertial dynamic system. Our attempt is to address the question of how the
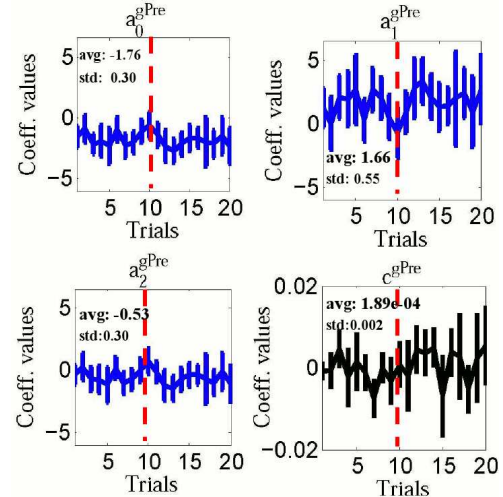

Fig. 4. The evolution of coefficients of the 3rd order auto regressive predictive controller of the guider.

follower's confidence towards the guider should be accounted for in designing a closed loop controller. Here, we argue that the confidence of the follower in any given context should be reflected in the compliance of his/her voluntary movements to follow the instructions of the guider. By modeling the impedance of the voluntary movement of the follower using a time varying virtual damped inertial system, we observe the variability of the impedance parameters - virtual mass and
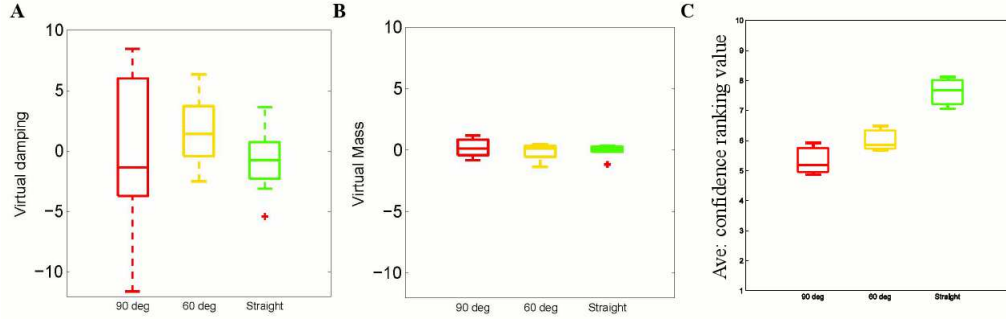
Fig. 6. Regression coefficients in Eq. (6) of different paths: (A) Virtual damping coefficient for paths: 90° turn, 60° turn, and straight path.The average values are 3.055, 1.605, and -0.586 for 90° turn, 60° turn. and straight path respectively. (B) Virtual mass coefficient for paths: 90° turn, 60° turn, and straight path. The average values are 2.066, -0.083, and 0.002 for 90° turn, 60° turn, and straight path respectively, (C) The follower's confidence: The confidence scale varies from 1 to 10 from the lowest to the highest. The average response value across straight, 60°, turn and 90° turn are shown with variability. The significance was computed by Mann-Whitney U test.

damping coefficients - in paths with different complexities (contexts). The three paths are shown in Fig. 1(D).

The experimental results of eight pairs of subjects in three types of paths - 90° turn, 60° turn, and a straight - are shown in Fig. 6. Here we extracted motion data within a window of 10 seconds around the 90° and 60° turns, and for fairness of comparison, we took the same window for the straight path for our regression analysis to observe the virtual damping coefficient and the virtual mass in three different paths. Fig. 6(A) shows the variability of the virtual damping coefficient, and Fig. 6(B) shows that of the virtual mass for the above three contexts. We can notice from Fig. 6(A) that the variability of the virtual damping coefficient is highest in the path with a 90° turn, with relatively less variability in that with a 60° turn, and least variability in the straight path. However, we do not notice a significant variability in the virtual mass across the three contexts.

In Fig. 6 the average values of the virtual mass distribution and the virtual damping coefficient in straight path are lowest. This shows that the confidence level of the follower is greater in the straight path. Furthermore, Table III and Table IV show the results of Mann Whitney U test for different paths (90° turn, 60° turn, straight path) of coefficients in Eq.6. Results in Table III show that the virtual damping coefficient in 90° turn was significantly different from that in straight path ($p < 0.01$). Moreover, virtual damping coefficient in 60° turn was also significantly different from that in straight path ($p < 0.02$). There was no statistically significant difference between the

virtual damping coefficient in path 90° turn and 60° turn ($p > 0.60$). Furthermore, the virtual mass distribution in Eq. (6) is shown in Fig. 6(B). Interestingly, only straight path was statistically significantly different from 90° turn ($p < 0.01$). However, the Mann Whitney U test in between 60° turn and straight path is not significantly different ($p > 0.70$). This may come from the fact that the follower has more confidence to follow the guider in a straight path than other two paths. Therefore these results confirm that the follower's confidence level is reflected in the time varying parameter of the virtual damped inertial system. We also note that the virtual damping coefficient is a more sensitive to predict the level of confidence than is virtual mass.

Human participants consistently confirmed that their confidence level to follow the guider dropped from the straight path to that with a 60° turn, to that with a 90° turn. Here, we show the average ranking value across the 8 pairs of follower for following the guider above three paths as shown in Fig. 6(C). The average ranking value is higher for straight path than 90° or 60° turns. However, average ranking value for 60° turn greater than 90° turn as shown in Fig. 6(C). The results confirm that the follower is more confident to follow the guider in straight path than 90° turn and 60° turn. This results agree with the virtual mass and virtual damping coefficient representation in Fig. 6(A) and Fig. 6(B)

TABLE III
VIRTUAL DAMPING COEFFICIENTS. STATISTICAL SIGNIFICANCE WAS COMPUTED USING THE MANN-WHITNEY U TEST.

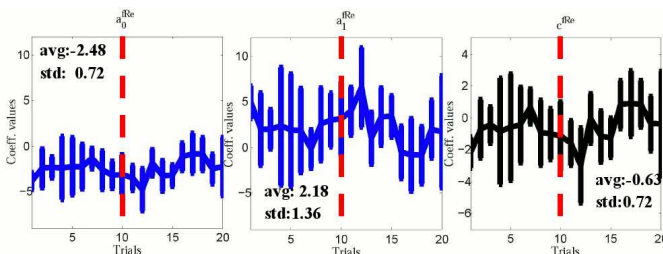| Paths	Mean	
90° turn	3.055	$p(90^0 turn \leftrightarrow 60^0 turn) > 0.6,$
60° turn	1.605	$p(60^0 turn \leftrightarrow Straight path) < 0.02^*,$
Straight path	-0.586	$p(90^0 turn \leftrightarrow Straight path) < 0.01^*$

Therefore, we conclude that the virtual damping coefficient can be a good indicator to control the push/pull behavior of an intelligent guider using a feedback controller of the form given in Eq. (6), where F(k) is the pushing/pulling tug force along the rein from the human guider at k^{th} sampling step, M is the time varying virtual mass, M_0 is its desired value, ζ is

Fig. 5. The evolution of coefficients of the 2nd order auto regressive reactive controller of the follower.

TABLE IV
VIRTUAL MASS. STATISTICAL SIGNIFICANCE WAS COMPUTED USING THE
MANN-WHITNEY U TEST.

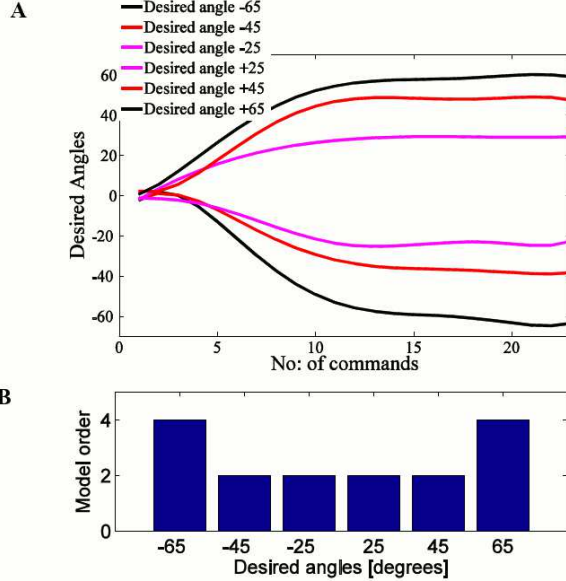| Paths	Mean	
90° turn	2.066	$p(90^0 turn \leftrightarrow 60^0 turn) > 0.8,$
60° turn	-0.083	$p(60^0 turn \leftrightarrow Straight\,path) > 0.7,$
Straight path	0.002	$p(90^0 turn \leftrightarrow Straight\,path) < 0.01^*$

Fig. 7. Validation of the guider's control policy: (A). completion of the reaching task. The desired angles are $-65°$, $-45°$, $-25°$, $+25°$, $+45°$, and $+65°$, (D) The average best fit model order selection across the subjects by using AIC for the above desired angles.

the time varying virtual damping coefficient, k is the sampling step, and ζ_0 is its desired value.

$$F(k+1) = F(k) - (M - M_0)\ddot{P}_f(k) - (\zeta - \zeta_0)\dot{P}_f(k) \quad (6)$$

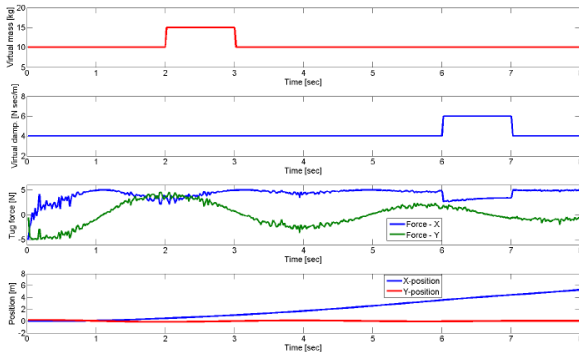Fig. 8. Simulation results: The tug force and position variation of the follower in order to sudden change of the virtual mass $M = 15$[kg] from $t = 2$s to $t = 3$s and the virtual damping coefficient $\zeta = 6$[Nsec/m] from $t = 6$s to $t = 7$s.

F. Validating the guider's control policy

G. Optimality of muscle recruitment

We show results of the validating the guider's control policy when it is implemented on the planar 1-DoF robotic arm. Here we show how the following error ϕ reduced over time across the trials across all subjects for 6 desired angles as shown in Fig. 7(A). Results show that guiding controller can bring human subjects into the desired angular positions and settle down in a reasonable time as shown in Fig. 7(A). Here Akaike Information Criterion (AIC) is used to find the best fit order of the polynomials [17] of the reaching curves in Fig. 7(A). To understand the optimal order of the polynomial, we show the average model order across the subjects for 6 desired angles in Fig. 7(B). The results show that the follower's behavior fits into 2nd order polynomial when the desired angles are $-45°$, $-25°$, $+25°$, and $+45°$. The test results again confirm that when the extracted guider's 3rd order control policy implemented on the robotic arm, it could bring the follower into the desired position and follower's behavior fits into 2nd order as we noticed followers model order from human demonstration experiments. However, for the higher desired angles ($-65°$ and $+65°$), the average model order is 4.

H. Developing a closed loop path tracking controller incorporating the follower's confidence level

Now we combine the guider's 3rd order predictive policy to control the swing movement of the hard rein, with the tug force modulation rule in Eq. 6 to form a complete controller that accounts for the state of the follower that indicates his/her confidence level.

We use the last 10 trials coefficients values as marked on Fig. 4 and 5 by red dashed line to calculate the statistical features of the regression coefficients in order to make sure the model reflects the behavior of the human participants at a mature learning stage. The model parameters were then found to be: $a_0 = N(-1.9216, 0.2590^2)$, $a_1 = N(2.0125, 0.4735^2)$, $a_2 = N(2.0125, 0.4735^2)$ and $c = N(-0.7429, 0.2416^2)$.

We conducted numerical simulation studies forming a closed loop dynamic control system of the guider and the follower using the control policy given in Eq. (2) together with virtual damped inertial model equation of the follower given in Eq. (6) to understand the variability of the virtual model parameters based on the model. We set the virtual mass $M = 15$[kg] from $t = 2$s to $t = 3$s and the virtual damping coefficient $\zeta = 6$[Nsec/m] from $t = 6$s to $t = 7$s to observe tug force variation in Eq. (6) as shown in Fig. 8(C). The tug force variation Fig. 8(C) shows that, the virtual damping coefficient more influenced to vary the tug force than the virtual mass. The results again suggest that virtual model parameter would be used to indicate the confidence of the follower.

To understand the optimality of muscles, we first study the responsibility assignment of muscles from EMG recordings, since the raw EMG data were contaminated with noise, we again used Wavelet Toolbox (The Math Works Inc) to extract the signal without noise. The raw EMG signal is a symmetrical envelope as shown in Fig. 9(A). It was suggested to adopt
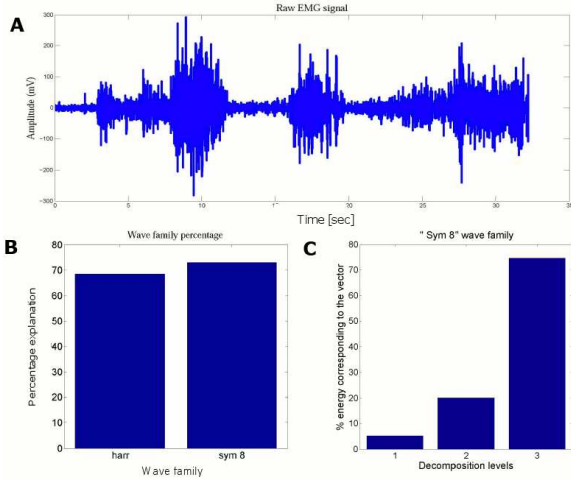
Fig. 9. Selection of wavelet family for EMG vector:(A) A representative raw EMG signal from Anterior Deltoid muscle of the guider, (B) Two wavelet families (harr, sym8) energy percentage representation of action vector of all subjects in all trials, (C) Vector containing the percentages of energy corresponding to the details of percentage energy of sym8.

the Symlets wave family (symmetrical sinusoidal wave) [14] for EMG analyzing. For clarity, we tested two types of wave families (harr and sym8) in Wavelet Toolbox as shown in Fig. 9(B) for all subjects over all trials. The percentage of energy corresponding to the approximation of sym8 (Symlets) and harr (Harr) values are 72.91% and 68.46% respectively as shown in 9 (B) by a bar chart. Therefore, we select sym8 (Symlets) for our symmetrical EMG wave analysis.

The percentage of energy corresponding to approximation for different decompression levels were found to be 99.52%, 95.97%, 92.05%, 85.41%, and 20.36% for decompression levels 3, 4, 5, 6 and 7 respectively. The highest percentage of energy was gained when the decompression level is 3. Next our attempt is to understand the percentages of energy corresponding to the 1 to 3 decomposition levels. Fig. 9(C) shows the percentage energy corresponding to the 1 to 3 decomposition levels of the EMG signal. Since the 3$^{\text{rd}}$ decomposition level has highest percentage energy level (76%), hereafter we use the 3$^{\text{rd}}$ decomposition level to analyze raw EMG data.

I. Behavior of individual muscles

In order to ascertain whether the low internal impedance control strategy converges to a minimum energy control solution, how does the individual muscle EMG vary over trials?. We plotted average normalized individual muscle over trials as shown in Fig. 10(A). We notice that the proportion of responsibility taken by the posterior Deltoid monotonically increases relative to the anterior Deltoid. Moreover, proportion of responsibility taken by the Biceps increases relative to the Triceps. This indicates that the above muscle pairs try to reduce co-activation in order to learn a low internal impedance control strategy. Therefore, this is in agreement with other studies that show a similar pattern of reduction in muscle co-contraction when motor learning progresses [18].

J. Behavior of pairs of antogonist muscles

We further analyzed the behavior of the averaged normalized EMG ratio between frontal and dorsal muscles over trials as shown if Fig. 10(B). The ratios of anterior and posterior muscles are decreased over trials in Fig. 10(B): M1 while ratio of Biceps and Triceps is increased in Fig. 10(B): M2. This suggests that, the priority muscle activation is taken by frontal and dorsal muscle of Deltoid than Biceps Triceps pair while the guiding agent produces movements in horizontal plane swing, anterior and posterior Deltoid pair is more activated to generate the tug forces along the hard rein.

K. Behavior of total EMG over trials

To compute the average EMG for all four muscles of all ten participants that reflects the average energy consumed in a trial given by $J = \sqrt{\sum_{i=1}^{4}\sum_{j=1}^{S_N} EMG_{ij}^2}$, where S_N is the number of subjects, EMG_{ij} is the average rectified EMG of the ith muscle of the jth participant. The behavior of this cost indicator J is shown in Fig. 10(C). We can clearly observe from the 2$^{\text{nd}}$ order best fit curve that J starting from lower- mid way of the training trials increase to a maximum - decreases in last 10 trials - reaches to minimum values at the last trial. This suggests that optimization is a non-monotonic process. During the first trials, it may have given priority to order selection than optimization in the actuation space, which is also reflected in the behavior of R^2 values in Fig. 3. Once the optimal order is selected, subjects exhibit monotonic optimization in the actuation space as seen in the last 10 trials of Fig. 10(C), with a corresponding increase of R^2 values in Fig. 3.

V. DISCUSSION

In this paper we present the characteristics of an optimal state dependent control policy found in human participants to guide a person with limited visual and auditory perception (follower) in an uncalibrated environment. If an intelligent agent (man/machine) is given the task to guide such a follower using only a hard rein, the guiding agent should learn a control policy that can effectively manage the variability of follower's behavior [19]. In this study, we conducted experiments to understand how two human participants interact with each other using haptic signals through a hard rein to achieve a path tracking goal when one partner was cut off from auditory and visual feedback from the environment (the follower), while the other (the person with environmental perception) gets full state feedback of the follower to find variability of movement and uncertainty of the behavior. The predictive and reactive policies of the guider and the follower in Fig. 3(A) and (C), showed that the R^2 values of the guider's predictive and follower's reactive behavioral policies increased over trials. The Mann Whitney U test results among different orders of autoregressive policies confirm that the guider's policy is best approximated by a 3$^{\text{rd}}$ order model while the follower's state transition policy is best approximated by a 2$^{\text{nd}}$ order model. Returning to the questions posed at the beginning of this study, it is now possible to state that the guider and the follower give more emphasis on predictive and reactive models
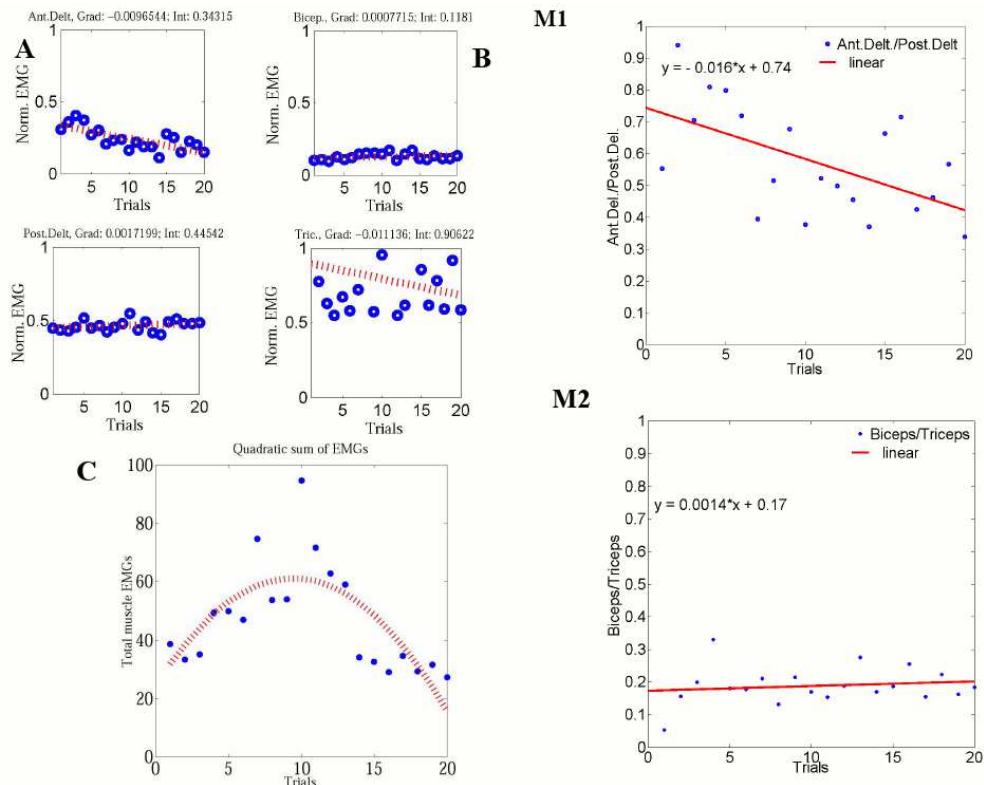
Fig. 10. The behavior of the average normalized muscle EMGs: (A) Average normalized muscle EMG anterior Deltoid, posterior Deltoids, Biceps, and Triceps. The gradient and intercept of individual muscles are (-0.005, 0.315), (0.004,0.426), (0.001, 0.133), and (-0.013, 0.995) for Anterior Deltoid, Posterior Deltoid, Biceps, and Triceps respectively. (B) Frontal and dorsal muscle ratio: M1- Biceps triceps muscle ratio, M2- anterior Deltoid posterior Deltoid muscle ratio. (C) The behavior of this cost indicator J of the 2nd order best fit curve for average EMGs of all four muscles of the ten subjects across trials.

respectively. This also accords with previous findings which showed that subjects learn both predictive and reactive models during different movements [20]. The different orders of the guider's predictive ($N = 3$) and the follower reactive ($N = 2$) policies suggest that in general, the guider depends on more historical information to generate an action, while the follower depends on less.

Variability is an indispensable feature in human behavior [21]. Therefore we moved on to understand the specific properties of variability of human guiding behavior in this particular task by observing the variation of polynomial coefficients in Eqs. (2) and (3) across trials. By modeling the control policy learned by the guiding agent as a discrete state dependent auto-regressive function, we found that guiding agent learns a stochastic stable control policy across 20 trials as shown in Figs. 4 and 5. These results are consistent with those of previous studies on stochastic human behavior [22], [23], [21] in similar contexts.

When the extracted guider's 3rd order control policy implemented on the robotic arm, it was able to bring the follower into the desired position as shown in Fig. 7(A) and follower's behavior fits into 2nd order as shown in Fig. 7(B) as we noticed followers model order from human demonstration experiments. However, we notice that followers model order fits for the model order 4 for higher desired angles like $-65°$ and $+65°$. This might come from the follower would not able to interpret the higher angles of turning.

Previous studies on human confidence on a helping agent have shown that humans tend to depend entirely on the helping agent when they are in hazardous environments [11] until sudden a change occurs [24]. This implies that the degree of compliance in a follower should drop if the follower loses confidence in the helping agent. By modeling the impedance of a follower as a virtual damped inertial system, we then considered the variability of the follower's impedance parameters (the virtual mass and damping coefficients) at different turn angles. From the three types of paths discussed in section IV (E), the blindfolded participants who played the role of the follower confirmed that their confidence in following the guider was highest in the straight path and it dropped in the other paths so that the confidence was medium in the path with a $60°$ turn, and least in that with a $90°$ turn. The results of virtual impedance parameters in Eq. (6) are shown in Fig. 6(A) and Fig. 6(B). Our experimental results of human participants also show that the variability of the virtual damping coefficients correlates more with the complexity of the path in Fig. 6 - reflecting the confidence level of the follower - than that of the virtual mass coefficient. Fig. 6 shows that the higher confidence of the follower in the straight path results in a lower average value of the virtual damping coefficient. When the follower drops his confidence in $90°$ turn and $60°$ turn, the guider has to exert a higher tug force to take following agent into desired trajectory that leads to higher average values for the virtual mass and virtual damping

coefficient.

Therefore, our results from human-human demonstrations provides useful design guidelines to human-robot interaction that should account for the real-time confidence and trust level of the human counterpart. In a human-robot interaction scenario such as a fire-fighter being guided by a robot through thick smoke, the estimate of the followers' confidence using the above method could be used to change acceleration/deceleration of the intelligent agent.

While learning the control policy, we next considered gradual change in muscle activation of the guider across the trials to see optimality of total effort to generate actions in the actuation space by the guider. Previous work [25] has proved that the total muscle activation for a single task decreased over their learning trials [25]. From the 2nd order best fit curve for the quadratic sum of EMG J for all muscles as shown in Fig. 10(C), we can observe that J increase to a maximum around the 10th trial and then decreases in last 10 trials. This suggests that effort optimization is a non-monotonic process. During the first 10 trials, participants may have given priority to order selection than optimization in the actuation space, which is also reflected in the behavior of R^2 values in Fig. 3. Once the optimal order is selected, subjects exhibit monotonic optimization in the actuation space as seen in the last 10 trials of Fig. 10(C), with a corresponding increase of R^2 values in Fig. 3. However, our observation on the guider's muscle activation gradually progresses from an initial muscle co-contraction based command generation strategy to a low energy policy with minimum muscle co-contraction. Therefore, this is in agreement with other studies that show a similar pattern of reduction in muscle co contraction when motor learning progresses [18]. This phenomenon can come from the fact that the guiding agent builds internal models [26] of hand and task dynamics to guide the blindfolded follower.

In the future, by combining the proposed control policy and the confidence studies, we will implement a full controller for guiding a human with limited auditory and visual perception from the environment. It will be interesting to numerically test whether construction of internal models of the follower's behavioral dynamics will lead to smoother and efficient model based controllers. This will also help us to implement a model based predictive controller in a robot to guide a human follower in a low visibility environment. The strength of this approach is that the robotic controller will be able to adjust to the changes of the behavioral dynamics of the human follower in varying distraction and stress conditions in a fire-fighting context.

In addition to applications in robotic guidance of a person in a low visibility environment, our preliminary findings shed light on the optimality criteria that the motor system would be using to apportion control responsibility across different muscles of a surgeon interacting with a robot to perform minimally invasive surgery. In that case, the robot could share a part of the responsibility of constructing internal models of interaction dynamics between the robot and tissues in various surgical tasks in order to accelerate the surgeon's reduction of muscle co-contraction [27]. Therefore, we will continue to discover a generic robotic learning strategy that can be generalized across robotic assisted surgery as well as robotic assisted guidance in low visibility environments.

REFERENCES

[1] J. Casper, & R. R. Murphy, "Human-robot interactions during the robot-assisted urban search and rescue response at the world trade center", *IEEE Transactions on Systems, Man, and Cybernetics, Part B*, vol.33(3), pp.367-385, 2003.

[2] A. Finzi & A. Orlandini, " A mixed-initiative approach to human-robot interaction in rescue scenarios", *American Association for Artificial Intelligence*, 2005.

[3] J. Penders et al. , "A robot swarm assisting a human firefighter", *Advanced Robotics*, vol 25, pp.93-117, 2011.

[4] J. R. Marston et al, "Nonvisual route following with guidance from a simple haptic or auditory display", *Journal of Visual Impairment & Blindness*, vol.101(4), pp.203-211, 2007.

[5] J. M. Loomis et al, "Navigation system for the blind: Auditory Display Modes and Guidance", *IEEE Transaction on Biomedical Engineering*, vol.7, pp. 163 - 203, 1998.

[6] A. A.Melvin et al, "'ROVI: a robot for visually impaired for collision-free navigation Allan Melvin ",*Proc. of the International Conference on Man-Machine Systems (ICoMMS 2009)*, pp. 3B5-1-3B5-6, 2009.

[7] I. Ulrich & J. Borenstein, "The GuideCane-applying mobile robot technologies to assist the visually impaired ",*Systems, Man and Cybernetics, Part A: Systems and Humans, IEEE Transactions*, vol. 31, pp. 131 - 136, 2001.

[8] S. Tachi et al "Electrocutaneous Communication in a Guide Dog Robot(MELDOG)", *IEEE Transaction on Biomedical Engineering*, vol.7, pp. 461 - 469, 1985.

[9] J. M. Loomis et al, "Navigating without vision: basic and applied research", *The journal of the American Academy of Optometry,Optometry & Vision Science*, Vol. 78(5), pp.282-289, 2001.

[10] Park, E, Quaneisha, J, & Xiaochun, J, "Measuring trust of human operators in new generation rescue robots" *Proceedings of the JFPS International Symposium on Fluid Power*, vol. 7, 2008.

[11] D.P. Stormont, "Analyzing human trust of autonomous systems in hazardous environments", *Proc. of the Human Implications of Human-Robot Interaction workshop at AAAI*, pp. 27-32, 2008.

[12] A.Freedy et al,"Measurement of trust in human-robot collaboration" , *IEEE International conference on Collaborative Technologies and Systems* , 2007.

[13] Hancock, P. A. et al, "A meta-analysis of factors affecting trust in human-robot interaction"', *The Journal of the Human Factors and Ergonomics Society*, vol.53(5), pp.517-527, 2011.

[14] Flanders.M, "Choosing a wavelet for single-trial EMG" ,*Journal of Neuroscience Methods*, vol.116.2, pp.165-177, 2002.

[15] Richardson, M. J., & Flash, T., " Comparing smooth arm movements with the two-thirds power law and the related segmented-control hypothesis"', *Journal of neuroscience*, 22(18), 8201-8211, 2002.

[16] H. M Christopher, & D.M.Wolpert, "Signal-dependent noise determines motor planning" *Nature*, vol. 394.6695, pp. 780-784, 1998.

[17] Akaike, H., "A new look at the statistical model identification", *IEEE Transactions on Automatic Control*, vol.19(6), pp.716-723, 1974.

[18] D.W. Franklin et al, "Adaptation to stable and unstable dynamics achieved by combined impedance control and inverse dynamics model" ,*Journal of neurophysiology*,vol.90, pp. 3270-3282,2003.

[19] V.Duchaine & C.Gosselin," Safe, stable and intuitive control for physical human-robot interaction", *IEEE International Conference on Robotics and Automation (ICRA) 09*, pp. 3383-3388, 2009.

[20] D.A. Nowak& J.Hermsdorfer, " Predictive and reactive control of grasping forces: on the role of the basal ganglia and sensory feedback", *journal of Experimental brain research*, vol.173(4), pp.650-660, 2006.

[21] N. Mitsunaga et al, "Robot behavior adaptation for human-robot interaction based on policy gradient reinforcement learning" , *Intelligent Robots and Systems(IROS 2005) IEEE/RSJ International Conference on. IEEE*, 2005.

[22] J.D.Sterman, " Deterministic chaos in models of human behavior: Methodological issues and experimental results"', *System Dynamics Review*, vol.4(12), pp.148-178, 1998.

[23] A.M.van Mourik et al, "Deterministic and stochastic features of rhythmic human movement", *journal ofBiological cybernetics*, vol.94(3), pp.233-244, 2006.

[24] G.Johannsen & W. B.Rouse, "Mathematical concepts for modeling human behavior in complex man-machine systems", *Human Factors: The Journal of the Human Factors and Ergonomics Society*,vol. 21(6),pp. 733-747, 1979.

[25] I.A.Stokes & M.M. Gardner , "Lumbar spinal muscle activation synergies predicted by multi-criteria cost function", *Journal of biomechanics* ,Vol. 34(6), pp.733-740, 2001

[26] K.A. Thoroughman & S. Reza. "Learning of action through adaptive combination of motor primitives" ,*Nature*, vol.407, pp. 742-747,2000.

[27] A. P. Kypson et al, "Robotic cardiac surgery", *Journal of Long Term Effects of Medical Implants*, vol. 13, pp. 451-464, 2003.

Jacques Penders Prof Jacques Penders joined Sheffield Hallam in 2003. Jacques was awarded an MEng in Landscape Architecture by RHSTL, Boskoop, The Netherlands, an MSc in Philosophy and an MSc in Mathematics by the University of Amsterdam, and a PhD in Artificial Intelligence by the University of Maastricht. He held a teaching position at the University of Amsterdam, and several research and (international) management positions at KPN Research. He has published in international journals and conference proceedings on the subjects of Swarm Robotics, Artificial Intelligence and Robotics, Multimedia retrieval and AI, Logistics and AI and on the Privacy aspects of Communication Traffic Data. Jacques's current research interest is in Natural Agents and Robotics, he currently pursues two tracks: - Exploring the basic fabric of group behavior by modeling groups of natural organisms and implementing groups of artificial agents, the latter includes swarm robotics and - Understanding the Communicational Landscape for tactile/haptic Human-Robot interaction.

Anuradha Ranasinghe Anuradha Ranasinghe is a PhD candidate in Laboratory for Morphological Computation and Learning at King's College London. Her research focuses on design and investigate haptic communicational interface between a human agent and a mobile robot guide. Her research interests are human-robot interactions, human's perceptions in haptic based guidance, and humans' motor control actions in moving. Her work nominated for the Franklin Taylor Memorial Award for the best paper and the Best Student Paper Award in IEEE SMC proceeding 2013. She worked as a Lecturer at KDU, UOM, Sri Lanka in Department of Electronics and Electrical. She received her B.Sc special degree in Physics from USJP, Sri Lanka and she worked on design an automated system for water purification plant.

Thrishantha Nanayakkara Thrishantha Nanayakkara received the BSc and MSc degrees in electrical engineering from the University of Moratuwa (UM), Sri Lanka (1996), and Saga University (SU), Japan (1998), and PhD in robotics from SU (2001). He was a postdoctoral research fellow in the department of biomedical engineering, Johns Hopkins University, USA, 2001-2003; a senior lecturer in the faculty of engineering at the UM; a Radcliffe Fellow at Harvard University, USA (2008/09), and a research affiliate at MIT (2008/09), USA. He is currently a senior lecturer in the department of Informatics, Kings College London. His research interests are in soft robotics, and robotic interaction with uncertain environments. He has published one textbook and more than 80 peer reviewed papers.

Prokar Dasgupta has been an Academic Urologist at Guys Hospital, London, U.K., since 2002. He is a pioneering robotic urological surgeon in the U.K. He is recognized internationally for the Guys robotic cystoprostatectomy technique. He also pioneered the minimally invasive method of delivering botulinum toxin to refractory overactive bladders named the Dasgupta technique. He has over 500 publications including over 100 peer-reviewed papers. Dr. Dasgupta has received 25 awards including the prestigious Jack Lapides Prize, the Geoffrey Chisholm Gold Medal, and the 2006 Karl Storz-Harold Hopkins Golden Telescope.

Kaspar Althoefer holds a Degree in electronic engineering from the University of Aachen, Aachen, Germany, and the Ph.D. degree in electronic engineering from Kings College London, London, U.K. He is currently a Professor of Robotics and Intelligent systems at King's College London and Head of the Center for Robotic Research (CoRe). His research interests are force and tactile sensors for medical applications, miniaturised optic-fibre-based sensing, medical robotics, flexible and continuum robots, and neuro-fuzzy sensor signal analysis and classification.